NANO LETTERS
pubs.acs.org/NanoLett

Sustained Mechanical Self-Oscillations in Carbon Nanotubes

Jeffrey A. Weldon, Benjamin Alemán, Allen Sussman, William Gannett, and Alex K. Zettl*

Department of Physics and Center of Integrated Nanomechanical Systems, University of California at Berkeley, and Materials Sciences Division, Lawrence Berkeley National Laboratory, Berkeley, California 94720

ABSTRACT The potential size and power benefits of resonant NEMS devices are frequently mitigated by the need for relatively large, high-frequency, high-power electronics. Here we demonstrate controllable, sustained self-oscillations in singly clamped carbon nanotubes operating with a single dc voltage supply, and we develop a model that predicts the required voltage on the basis of the material properties and device geometry. Using this model, we demonstrate for the first time top-down, self-oscillating NEMS devices suitable for large-scale integration.

KEYWORDS Carbon nanotubes, oscillators, self-oscillation, NEMS, field emission

Nanoelectromechanical systems[1] (NEMS) based on vibrating mechanical elements have demonstrated excellent performance for many applications including chemical sensing,[2−4] mass sensing,[5] and high-frequency signal generation.[6] Although the mechanical element in these systems is on the nanoscale, significantly larger external components, typically high-frequency signal sources,[7,8] amplifiers, and integrated circuits,[6] are needed to drive the oscillations. An important step toward realizing truly nanoscale integrated systems is the reduction of the dependence on such external components. We report the achievement of controllable self-oscillations in isolated, singly clamped field-emitting carbon nanotubes (CNTs) driven only by a single dc bias voltage. A model is developed that correctly predicts the onset of self-oscillations in terms of device geometry and material properties. Using the model, we design and construct top-down, low-voltage, self-oscillating NEMS devices suitable for large-scale integration.

Passive resonators, by definition, require high-frequency signal sources to drive oscillations. Active oscillators do not necessitate a high-frequency signal source, but they do require active feedback circuitry to achieve oscillations. In the case of resonant NEMS devices, the desired size and power benefits are invariably offset by the bulky control electronics required for oscillation. A number of self-oscillation approaches have been explored.[6,9,10] Recent observations of oscillations in nanowires[11] are encouraging, but there is unfortunately neither a clear understanding of the underlying drive mechanism nor the requisite geometry to enable reliable, self-oscillation-based NEMS devices. We here elucidate the requisite geometry for NEMS self-oscillators, and our quantitative model establishes comprehensive design parameters for scalable devices.

We employ a singly clamped, cantilevered field-emitting[5,11,12] carbon nanotube in vacuum as a prototypical oscillator element, as shown schematically in Figure 1. When a sufficiently high dc bias is applied between the nanotube and a nearby counterelectrode, self-oscillations are initiated. A critical feature in achieving reliable self-oscillations is the angle between the nanotube's longitudinal axis and the counterelectrode: a nanotube oriented parallel to the surface can self-oscillate whereas one oriented perpendicular to the surface cannot. A transmission electron microscope (TEM) image of a multiwalled carbon nanotube attached to a conducting atomic force microscope tip and oriented parallel to an electrode surface is shown in Figure 2. As the bias voltage is increased from zero, the nanotube bends toward the counter electrode (Figure 2a,b) and field emission[13,14] occurs. Subsequent increases in the bias voltage result in an increase in the field emission current (∼0.1−1 μA), and above a critical, device-specific bias threshold or onset voltage V_o, sustained self-oscillations occur. Figure 2c shows a TEM image of a vibrating nanotube biased beyond V_o into the continuous self-oscillation mode. Because of the high

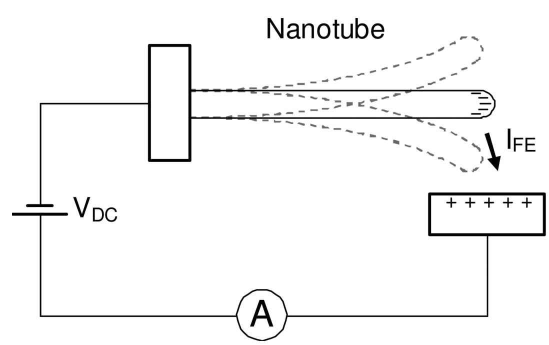

FIGURE 1. Schematic of the setup used to test self-oscillations in carbon nanotubes. A dc bias voltage is applied between the nanotube and the counter electrode, causing field emission from the nanotube to the counter electrode. An ammeter is used to measure the field-emission current.

* Corresponding author. E-mail: azettl@berkeley.edu.
Received for review: 01/15/2010
Published on Web: 04/22/2010

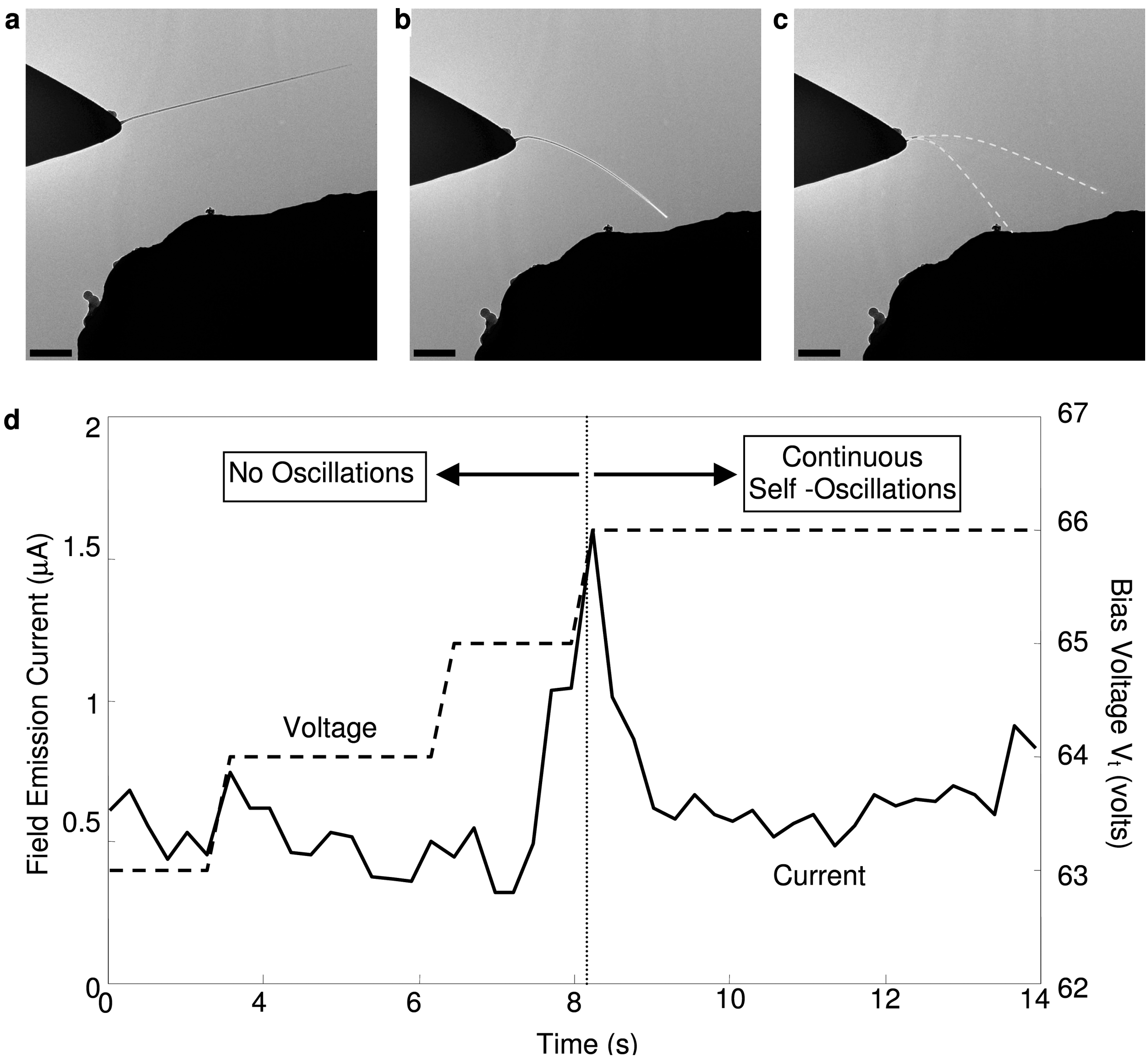

FIGURE 2. TEM images and experimental data during self-oscillation experiments. (a) TEM image of the nanotube with zero bias voltage. (The scale bar is 0.5 μm.) The nanotube is approximately 2.8 μm long. (b) TEM image of the nanotube with a bias voltage. The nanotube is charged and the electrostatic force draws the nanotube closer to the counter electrode. (c) TEM image of a self-oscillating nanotube. The nanotube is not easily visible while it is vibrating; the dashed lines, which delineate the vibrational amplitude, have been added for clarity. Although the nanotube appears to touch the counter electrode, it does not. The vibrational plane is located behind the visible edge of the counter electrode. (d) Field-emission current and applied bias voltage shown as a function of time. The nanotube begins sustained self-oscillations when the voltage is raised to 66 V. At this point, a large current spike starts continuous self-oscillations.

frequency of the vibrations (~4 MHz), the image of the nanotube is blurred and only the oscillation envelope (highlighted for clarity) is observable. (A movie showing the onset of sustained self-oscillations can be found in the Supporting Information.) A plot of field-emission current and applied voltage over time for the same device driven through V_o (= 65 V) is shown in Figure 2d. These data illustrate an important and consistent observation in our experiments: the onset of self-oscillations is associated with a current spike at V_o. We remark that the data in Figure 2d have been acquired using a low sampling rate; hence the response signal is coarse-grained and does not directly reflect the oscillatory response for $V_t > V_o$. In addition, confirmation of the oscillation was achieved visually in the transmission electron microscope. It is expected that the field-emission current would contain a substantial ac signal generated by the vibrating nanotube. However, bandwidth constraints, because of the large parasitic capacitance in our experimental setup, limited direct electrical detection. To experimentally determine the resonance frequency, the nanotube was biased just below V_o and the resonance frequency was found by applying an external ac signal.

We first examine the fundamental mechanism of self-oscillations in cantilevered, field-emitting nanotubes (or similar nanostructures). We then develop a detailed model that takes nanotube and electrode geometry into account. Using the predictive power of the model, we design and fabricate, using a top-down approach, scalable self-oscilla-

DOI: 10.1021/nl100148q | *Nano Lett.* **2010,** *10,* 1728--1733

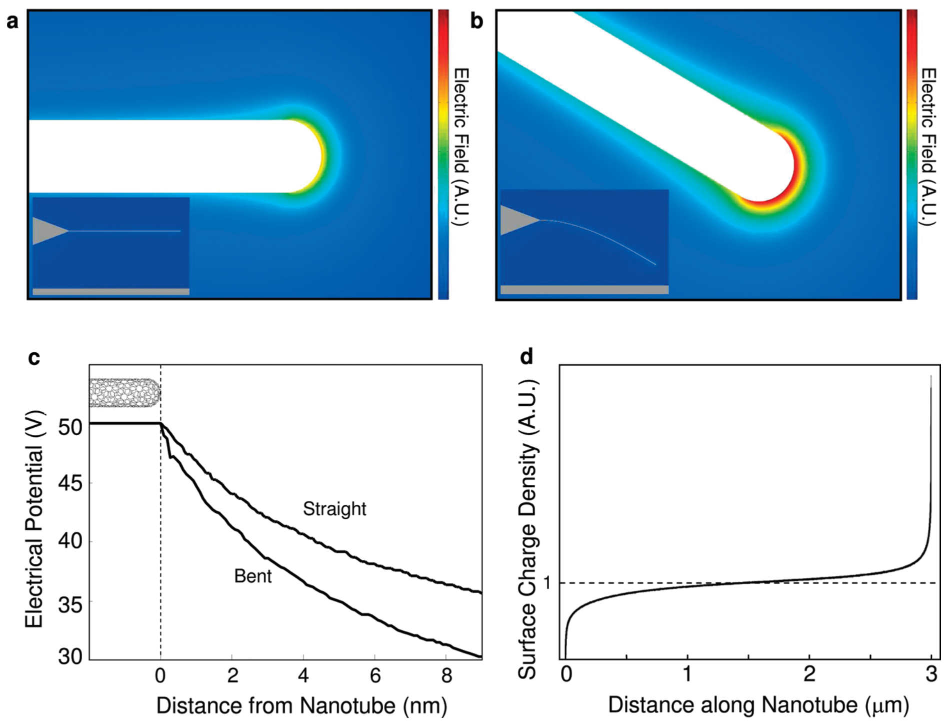

FIGURE 3. Simulations of the electrostatic properties of a 3-μm-long, 5-nm-radius carbon nanotube biased at 50 V. The nanotube is 1.5 μm from the counter electrode, shown in gray. (a) Electric field of a straight carbon nanotube. The electric field is enhanced at the tip of the nanotube by the increased curvature. (b) Electric field of the nanotube as it is bent close to the counter electrode. Notice that electric field at the tip is significantly larger than the field at the tip of the straight tube. (c) Electrostatic potential energy landscape near the tip of the nanotube. The barrier for field emission is substantially smaller for the bent tube, indicating that the field-emission current will be larger. (d) Surface charge density showing the distribution of charge over the length of the nanotube. The charge can be approximated as that of an infinitely long cylinder, shown by the dotted line, and a concentrated tip charge.

tion NEMS devices with an engineered oscillation frequency and turn-on voltage.

The nature of the self-oscillations can be understood qualitatively by examining the forces acting on the nanotube and the effect of these forces on the field-emission current. When the nanotube is biased below V_o, it is attracted to the counter electrode by the electrostatic force resulting from charge accumulations on the nanotube and the counter electrode. This attractive force is balanced by the repulsive mechanical restoring force of the bent nanotube cantilever. As is observed experimentally, vibrations begin when a burst of electrons discharges from the nanotube. This rapid discharge temporarily reduces the attractive electrostatic force; consequently, the mechanical restoring force suddenly dominates. Because of the significant resistance and capacitance of the system, there is a time delay in recharging the nanotube, and thus the nanotube is quickly pulled away from the counter electrode. The steplike forcing function initiates nanotube mechanical vibrations. The rapid discharge of electrons is analogous to the plucking of a guitar string. However, in the case of the nanotube, the vibrations are sustained indefinitely because the cycle of rapid discharge and repulsion (i.e., the plucking) repeats itself, much like the continuous strumming of a guitar string.

Another important aspect of sustained oscillators, such as more traditional inductor-capacitor based oscillators, is the presence of a limit cycle. Regardless of the initial condition, an oscillator with a limit cycle will converge to the same amplitude and frequency. In this work, the experimental evidence suggests that the nanotube oscillator does have a limit cycle. The frequency of oscillation is determined by the flexural resonance of the nanotube, which is a function of the material properties and the tension. The amplitude is a function of the field-emission current and the discharging times, suggesting a well-defined amplitude, which is in agreement with the experimental results.

We now turn to a closer examination of field emission from cantilevered and mechanically flexed nanotubes. This serves to explain the origin of the current spike that initiates self-oscillations and allows us, on the basis of geometrical device parameters alone, to predict the onset voltage for self-oscillations. Field emission occurs when electrons tunnel through the potential barrier near an object's surface into a nearby vacuum.[13,14] The tunneling current is greatly enhanced in 1D structures, such as nanotubes[15] because of higher local electric fields found at their tips. Figure 3a shows a finite-element simulation of the field of a straight nanotube near a flat, conducting electrode. The increased field at the tip is clearly evident. Figure 3b shows the field of the same nanotube bent toward the counter electrode. The field near the tip significantly increases as the distance to the counter electrode is reduced. This increased field leads to a reduced

DOI: 10.1021/nl100148q | *Nano Lett.* **2010,** *10,* 1728--1733

potential barrier at the tip, as shown in Figure 3c, which in turn causes the field-emission current to increase as the tube nears the counter electrode. The current spike associated with the onset of self-oscillations is caused by the nanotube quickly moving closer to the counter electrode. This rapid movement can be quantified by analyzing in greater detail the total force acting on the nanotube.

The electrostatic forces acting on the nanotube are primarily capacitive in nature. To model the capacitive force accurately, we employ finite element methods to simulate the surface charge density of a biased nanotube (Figure 3d.) Guided by this simulation, we approximate the total charge as the combination of a sidewall charge and a tip charge. We approximate the sidewall charge as that of an infinitely long cylinder (dashed curve in Figure 3d) and use standard techniques[16] to solve for the capacitive sidewall force.[17,18]

$$F_s(x, V_t) = \frac{\pi \varepsilon_0 L \sin\theta}{\sqrt{(d_0 - \frac{x}{2})((d_0 - \frac{x}{2}) + 2r)}\operatorname{arccosh}^2\left(1 + \frac{d_0 - \frac{x}{2}}{r}\right)} V_t^2 \tag{1}$$

Here, x is the displacement of the nanotube tip, d_0 is the initial distance (i.e., when $V_t = 0$) from the tip to the counter electrode, L is the length of the nanotube, r is the nanotube radius, V_t is the voltage of the nanotube with respect to the counter electrode, θ is the initial angle that the longitudinal axis of the tube makes with the normal to the ground plane, and ε_0 is the permittivity of vacuum. The tip charge is approximated with a parametrically derived expression for flat-end nanocylinders[19] modified to account for the closed end of the nanotube,[20] resulting in the electrostatic force acting on the tip of the nanotube:

$$F_t(x, V_t) = \frac{0.85\pi \varepsilon_0 ((d_0 + r)^2 r)^{1/3} \sin\theta}{2\sqrt{(d_0 - x)((d_0 - x) + 2r)}\operatorname{arccosh}^2\left(1 + \frac{d_0 - x}{r}\right)} V_t^2 \tag{2}$$

The elastic response of the nanotube is given by two components corresponding to the applied sidewall and tip forces. The resulting spring constants associated with the electrostatic sidewall and the tip forces are, respectively, $k_s = (8EI)/(L^3) = (8\pi E r^4)/(4L^3)$ and $k_t = (3EI)/(L^3) = (3\pi E r^4)/(4L^3)$, where E is the Young's modulus ($E \approx 1$ TPa[21] for a carbon nanotube) and $I \approx \pi r^4/4$ is the areal moment of inertia.

Equations 1 and 2 govern the rapid nanotube deflection that initiates self-oscillations. The equilibrium tip deflection $x = (F_s)/(k_s) + (F_t)/(k_t)$ is plotted in Figure 4a for selected values of initial tip−counter electrode separation d_o. The plots reveal that the tip position becomes unstable at a critical voltage, identified by the vertical lines in Figure 4a. At this

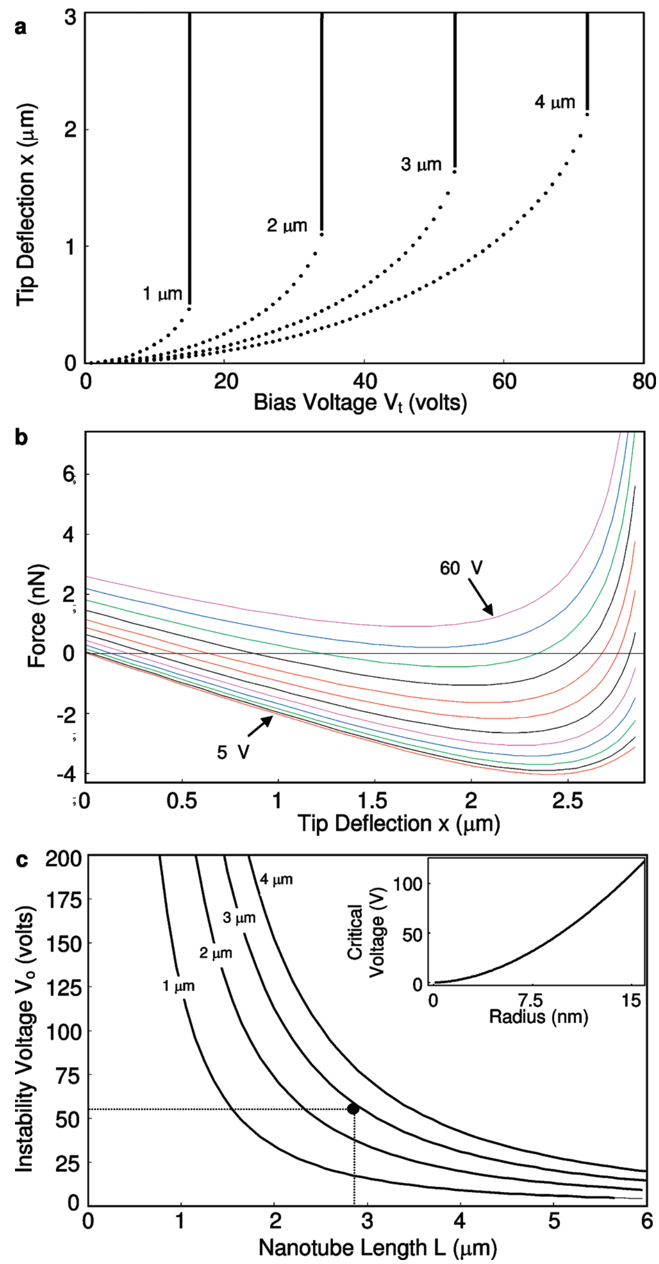

FIGURE 4. Electromechanical modeling of self-oscillating carbon nanotubes. (a) Equilibrium deflection of a 10-nm-radius nanotube tip as a function of the bias voltage shown for a tube of 3 μm length at various initial tip−surface distances (1, 2, 3, and 4 μm.) The vertical lines for each curve represent the voltage at which no equilibrium deflection exists for the tube and the tube becomes unstable. (b) Sum of the electrostatic and elastic forces as a function of the nanotube tip position for varying bias voltages (5−60 at 5 V intervals). Stable equilibrium positions are given by the first zero of each curve and increase, as expected, with increasing voltage but do not exist for the 55 and 60 V curves. (c) Nanotube instability voltages for varying tube lengths and initial tip−surface distances (1, 2, 3, and 4 μm). The inset shows how the instability voltage increases with tube radius for a tube with a length and an initial tip−surface distance of 3 μm. θ = 90° in all cases.

critical voltage V_o, the attractive electrostatic force overwhelms the repulsive elastic force and the nanotube is rapidly drawn to the counter electrode. This runaway deflec-

DOI: 10.1021/nl100148q | *Nano Lett.* **2010,** *10,* 1728–1733

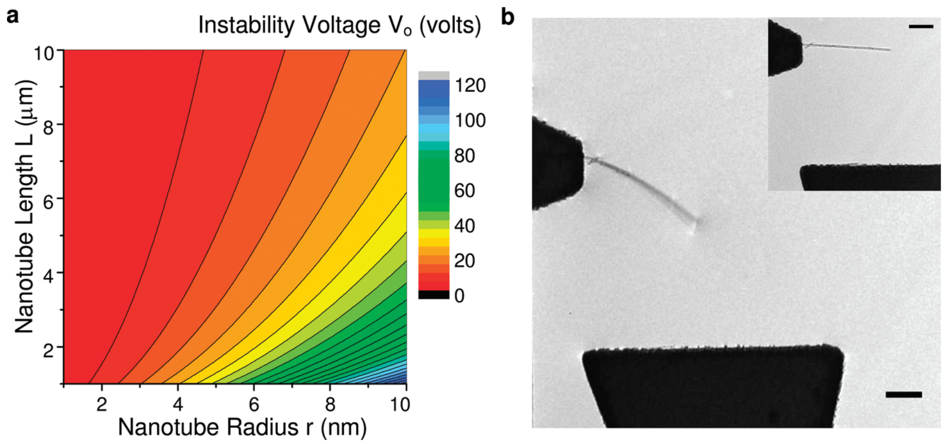

FIGURE 5. Geometric design landscape and fabrication of carbon nanotube NEMS oscillators. (a) Contour plot of the self-oscillation onset voltage given for $L = d_0$ ranging from 1 to 10 μm and for r between 1 and 10 nm. (b) Top-down carbon nanotube NEMS oscillator demonstrating sustained self-oscillations at 40 V; the inset shows the nanotube at 0 V. (The scale bar is 1 μm.)

tion has been previously observed in NEMS switches,[22,23] but here the nanotube is positioned such that it cannot reach the counter electrode.

The critical voltage V_o at which the nanotube position becomes unstable and self-oscillations commence can be evaluated directly from geometric device parameters (r, L, d_0, and θ). A plot of the total force (sum of eqs 1 and 2 and an effective spring force based on k_t and k_s) is shown in Figure 4b as a function of nanotube length L and for bias voltages V_t ranging from 5 to 60 at 5 V intervals. The first zero of each curve corresponds to the stable equilibrium deflection of the nanotube for a given V_t; this equilibrium deflection increases with increasing voltage. The instability voltage, V_o, of the system is given by the lowest voltage for which no zero exists and can be calculated by finding a V_t such that $F(x, V_t) > 0$ for all x. Such calculations were performed numerically on a 10-nm-radius tube, and the results are shown in Figure 4c for continuous values of tube length and several fixed initial tip−counter electrode distances. The inset of Figure 4c illustrates the behavior of the instability voltage with varying nanotube radius. In general, V_o increases for shorter tubes, larger tube radii, and larger initial tip− counter electrode distances. As an example, for the device geometry shown in Figure 3, the model predicts $V_o \approx 55$ V, which, given the uncertainty in the position of our bottom-up devices and the approximations of the model, is in excellent agreement with the experimentally observed $V_o = 66$ V.

Sustained self-oscillations will occur for applied bias voltage $V_t > V_o$ but only if the decay time for mechanical oscillations, given by $2Q/\omega_0$ where Q is the quality factor and ω_0 is the natural frequency of oscillation, is greater than or on the order of the recharging time, given by the RC time constant of the circuit. For the experiments described above, we estimate $2Q/\omega_0 \approx 10^{-4}$ and $RC \approx 10^{-5}$, consistent with our interpretation of the model. We note further that if the system is biased very close to but just below V_o then fluctuations (such as those associated with field-emission current noise) can temporarily kick the system into self-oscillation mode. Although such oscillations may last for several seconds, they are not sustainable.

Bottom-up fabricated self-oscillating devices such as those described above are extremely useful test structures, but their tedious serial assembly process gives them limited practical value. Because our model explicitly outlines the role that geometric parameters play in self-oscillations, it facilitates the engineering of self-sustaining NEMS oscillators amenable to large-scale fabrication. Figure 5a summarizes the geometric requirements (assuming $L = d_0$) for designing self-oscillating cantilevered devices that operate within a certain desired dc bias voltage range. For example, the graph indicates that a 10-μm-long carbon nanotube will self-oscillate for an applied bias $V_t \geq 10$ V if $r < 7$ nm whereas a 1-μm-long tube will oscillate for similar values of V_t if $r < 2.5$ nm.

We now employ scalable methods to fabricate fully integrated self-oscillating NEMS structures with predetermined performance characteristics. We use standard optical and electron-beam lithography, microfabrication processing, and simple nanotube deposition techniques (spin casting) to produce fully suspended nanotube-based oscillators with well-defined L, d_0, r, and θ. The inset of Figure 5b shows a TEM micrograph of an unbiased device composed of a suspended multiwalled carbon nanotube and a lithographically defined counter electrode. Figure 5b shows the same device biased into self-oscillations. For this device, V_o was determined experimentally to be 40 V, which agrees to within 10% of model predictions. The device architecture shown in Figure 5b was chosen to facilitate TEM characterization and was realized by performing all processing on a thin Si_3N_4 membrane that was then etched to produce the suspended structure. Of course, much simpler membrane-free approaches are possible that suspend nanotubes over trenches[24] and that exploit techniques for the controlled placement of highly aligned SWCNTs[25] or MWCNTs.[26]

DOI: 10.1021/nl100148q | Nano Lett. 2010, 10, 1728--1733

In summary, we have demonstrated controllable, sustained self-oscillations with carbon nanotube NEMS. Furthermore, we have used an electromechanical model to develop a comprehensive understanding of this behavior and have described the parameters necessary for designing proper device architectures. In addition, the model that we presented is a general model that can be applied to other materials such as nanowires and graphene and is likely applicable to previous observations of self-oscillation.[11] With these design parameters, we have fabricated operational top-down devices. The successful top-down fabrication of NEMS self-oscillators has important implications for future highly integrated, chip-based systems such as sensors,[5] logic and memory elements,[6] and high-frequency NEMS switches,[23] which can in principle be tailored to operate at dc bias voltages of less than 10 V.

Acknowledgment. We thank Ç. Girit, K. Kim, W. Regan, and M. Schriver for useful discussions and S. Onishi for technical assistance. This work was supported in part by the Director, Office of Energy Research, Office of Basic Energy Sciences, Materials Sciences and Engineering Division, of the U.S. Department of Energy under contract no. DE-AC02-05CH11231, which provided for detailed TEM characterization and device microfabrication (W.G.), and by the National Science Foundation within the Center of Integrated Nanomechanical Systems under grant EEC-0425914, which provided for the design, initial construction, and modeling of the oscillator (J.A.W., B.A., and A.S.). B.A. acknowledges support from the UC Berkeley Anselmo John Macchi Fellowship Fund in the Physical Sciences. Author contributions: J.A.W. conceived of and designed the experiments. J.A.W. and B.A. performed the experiments. A.S. performed finite-element simulations. B.A. developed the model. J.A.W. and B.A. interpreted the model and simulation results. B.A. conceived of and fabricated the top-down devices with assistance from J.A.W. and W.G., JA.W., B.A., and A.Z. cowrote the manuscript. A.Z. served as project PI.

Supporting Information Available. High-resolution TEM movie of the onset of self-oscillations corresponding to the data shown in Figure 2. Detailed explanation of the methods used in this work.This material is available free of charge via the Internet at http://pubs.acs.org.

REFERENCES AND NOTES

(1) Craighead, H. *Science* **2000**, *290*, 1532–1535.
(2) Wan, Q.; Li, Q.; Chen, Y.; Wang, T.; He, X.; Li, J.; Lin, C. *Appl. Phys. Lett.* **2004**, *84*, 3654–3656.
(3) Waggoner, P.; Craighead, H. *Lab Chip* **2007**, *7*, 1238–1255.
(4) Li, M.; Tang, H.; Roukes, M. *Nat. Nanotechnol.* **2007**, *2*, 114–120.
(5) Jensen, K.; Kim, K.; Zettl, A. *Nat. Nanotechnol.* **2008**, *3*, 533–537.
(6) Feng, X. L.; White, C. J.; Hajimiri, A.; Roukes, M. L. *Nat. Nanotechnol.* **2008**, *3*, 342–346.
(7) Unterreithmeier, Q.; Weig, E.; Kotthaus, J. *Nature* **2009**, *458*, 1001–1004.
(8) Mahboob, I.; Yamaguchi, H. *Nat. Nanotechnol.* **2008**, *3*, 369–369.
(9) Durand, C.; Casset, F.; Renaux, P.; Abele, N.; Legrand, B.; Renaud, D.; Ollier, E.; Ancey, P.; Ionescu, A.; Buchaillot, L. *IEEE Electron Device Lett.* **2008**, *29*, 494–496.
(10) Sekaric, L.; Zalalutdinov, M.; Turner, S.; Zehnder, A.; Parpia, J.; Craighead, H. *Appl. Phys. Lett.* **2002**, *80*, 3617–3619.
(11) Ayari, A.; Vincent, P.; Perisanu, S.; Choueib, M.; Gouttenoire, V.; Bechelany, M.; Cornu, D.; Purcell, S. *Nano Lett.* **2007**, *7*, 2252–2257.
(12) Jensen, K.; Weldon, J.; Garcia, H.; Zettl, A. *Nano Lett.* **2008**, *8*, 374–374.
(13) Gomer, R. *Field Emission and Field Ionization*; Harvard University Press: Cambridge, MA, 1961.
(14) Fursey, G. In *Field Emission in Vacuum Microelectronics*; Brodie I., Shwoebel P., Eds.; Kluwer Academic/Plenum Publishers: New York; 2005.
(15) Deheer, W. A.; Chatelain, A.; Ugarte, D. *Science* **1995**, *270*, 1179–1180.
(16) Jackson, J. D. *Classical Electrodynamics*, 3rd ed.; Wiley: New York, 1999.
(17) Hayt, W. H.; Buck, J. A. *Engineering Electromagnetics*, 7th ed.; McGraw-Hill Higher Education: Boston, 2006.
(18) Dequesnes, M.; Rotkin, S.; Aluru, N. *Nanotechnology* **2002**, *13*, 120–131.
(19) Ke, C.; Espinosa, H. *J. Appl. Mech.* **2005**, *72*, 721–725.
(20) Keblinski, P.; Nayak, S. K.; Zapol, P.; Ajayan, P. M. *Phys. Rev. Lett.* **2002**, *89*, 255503-1–255503-4.
(21) Wong, E. W.; Sheehan, P. E.; Lieber, C. M. *Science* **1997**, *277*, 1971–1975.
(22) Ke, C. H.; Espinosa, H. D. *Appl. Phys. Lett.* **2004**, *85*, 681–683.
(23) Ke, C. H.; Espinosa, H. D. *Small* **2006**, *2*, 1484–1489.
(24) Peng, H. B.; Chang, C. W.; Aloni, S.; Yuzvinsky, T. D.; Zettl, A. *Phys. Rev. B* **2007**, *76*, 035405-1–035405-5.
(25) Huang, L. M.; White, B.; Sfeir, M. Y.; Huang, M. Y.; Huang, H. X.; Wind, S.; Hone, J.; O'Brien, S. *J. Phys. Chem. B* **2006**, *110*, 11103–11109.
(26) Yuzvinsky, T. D.; Fennimore, A. M.; Kis, A.; Zettl, A. *Nanotechnology* **2006**, *17*, 434–438.

DOI: 10.1021/nl100148q | *Nano Lett.* **2010,** *10,* 1728--1733